Electronic Supplementary Material (ESI) for RSC Advances.

Supplementary Materials: Phase-change-induced martensitic deformation and slip system in GeSbTe

Moon Hyung Jang[*†‡], Kwang Sik Jeong[*‡], Seung Jong Park[*], Sung Jin Park[*], Mann-Ho Cho[*§], Jae Yong Song[¶]

[*]*Institute of Physics and Applied Physics, Yonsei University, Seoul, 120-749, Republic of Korea*

[¶]*Center for Nanocharacterization, Korea Research Institute of Standards and Science, Daejeon, 305-340, Republic of Korea*

[†]Current affiliation: Department of Electrical and Computer Engineering, University of Massachusetts, Amherst, MA 01003, USA

[§]To whom correspondence should be addressed. E-mail: mh.cho@yonsei.ac.kr

[‡]M.H.J. and K.S.J. contributed equally to this work.

Supplementary Figure Captions

Figure S1. HRTEM image of an as-grown GST film with no crystallized regions.

Figure S2. (a) HRTEM images of the monoclinic phase, which has an FCC angle of 90°, after annealing at 220 °C. (b) Corresponding FFT diffraction patterns of this crystal, showing γ of 80.7° and monoclinic (200) and (020) lattice spacings of 3.06 and 2.99 Å, respectively. (c) HRTEM image of another monoclinic phase, showing an FCC angle of 90°, after annealing at 220 °C. (d) FFT diffraction patterns obtained from the crystal shown in (c), showing γ of 81.0° and monoclinic (200) and (020) lattice spacings of 3.18 and 3.10 Å, respectively.

Figure S3. (a) HRTEM images of the monoclinic phase, which has an FCC angle of 90°, after annealing at 220 °C. (b) Corresponding FFT diffraction patterns of this crystal, showing γ of 81.1° and monoclinic (200) and (020) lattice spacings of 3.03 and 3.02 Å, respectively. (c) HRTEM image of another monoclinic phase, showing an FCC angle of 90°, after annealing at 220 °C. (d) FFT diffraction patterns from the crystal shown in (c) with a γ angle of 87.8° and monoclinic (200) and (020) lattice spacings of 3.18 and 3.00 Å, respectively.

Figure S4. Volume shrinkage (δv) of the crystallized region of radius R_a within an amorphous matrix of radius R_b. The crystallized region and the amorphous matrix are concentrically spherical in shape.

Figure S5. Images of the geometrically optimized 4**a**×4**b**×4**c** GST structure with deformation angles (γ) of (a) 86°, (b) 78°, (c) 74°, and (d) 66°, which have the same configurations as those shown in Figs. 4(c)–(e). The red-dashed boxes correspond to a 2**a**×2**b** cell of the GST structure.

Figure S6. (a) HRTEM images of FCC crystal with slip system in the FCC (111) plane along the $[\bar{1}10]$ direction. (b) Corresponding Fourier-transformed diffraction patterns, showing FCC[100] and FCC[010] interplanar spacings of 2.99 and 3.07 Å, respectively, and an angle of 88.6° between these planes. (c) Side view of successive atomic motion in the FCC crystal during slip along $[\bar{1}10]$ in the (111) plane from 1 to 10. The green arrow indicates the direction of the slip.

Figure S7. Total DOS of GST materials for various values of γ ranging from 90 to 66°, as obtained by VASP simulation. The vertical dotted line indicates the Fermi level (E_F) of the DOS.

The gap below E_F at 90° indicates the semimetallicity of the FCC crystal structure. After deformation, this gap is filled by electron states except at the angle of 70°.

Figure S1

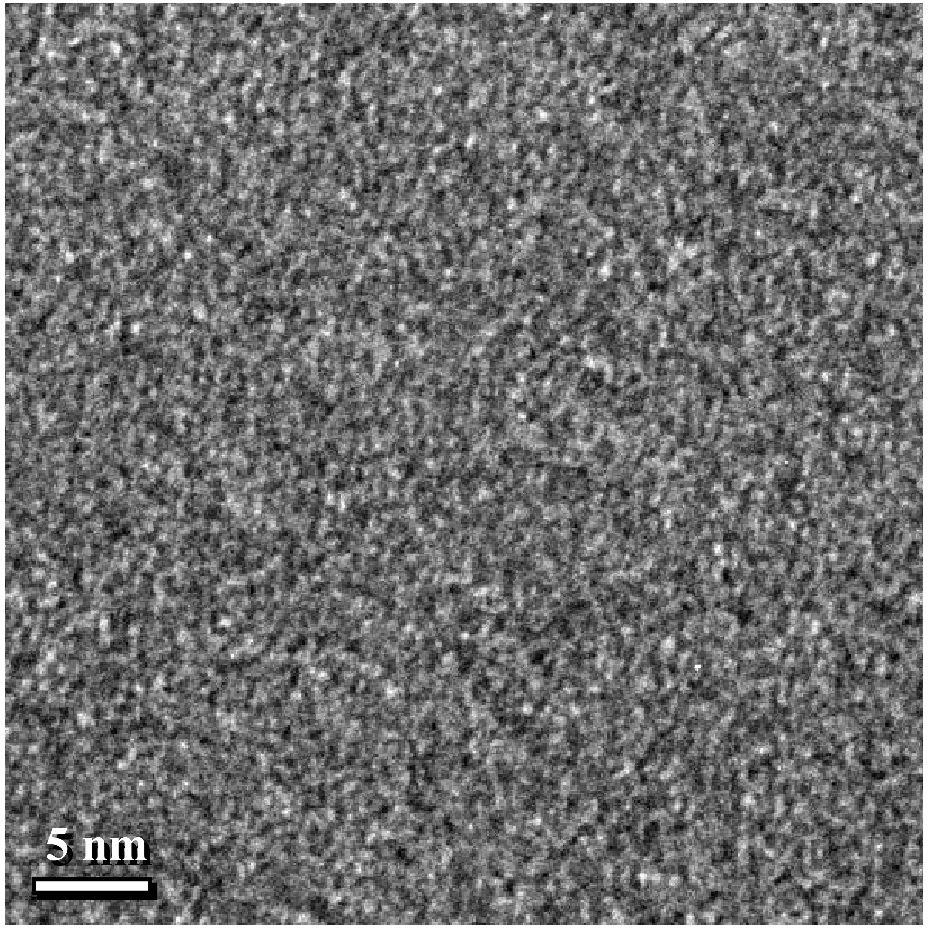

Fig. S1 Jang *et al*.

Figure S2

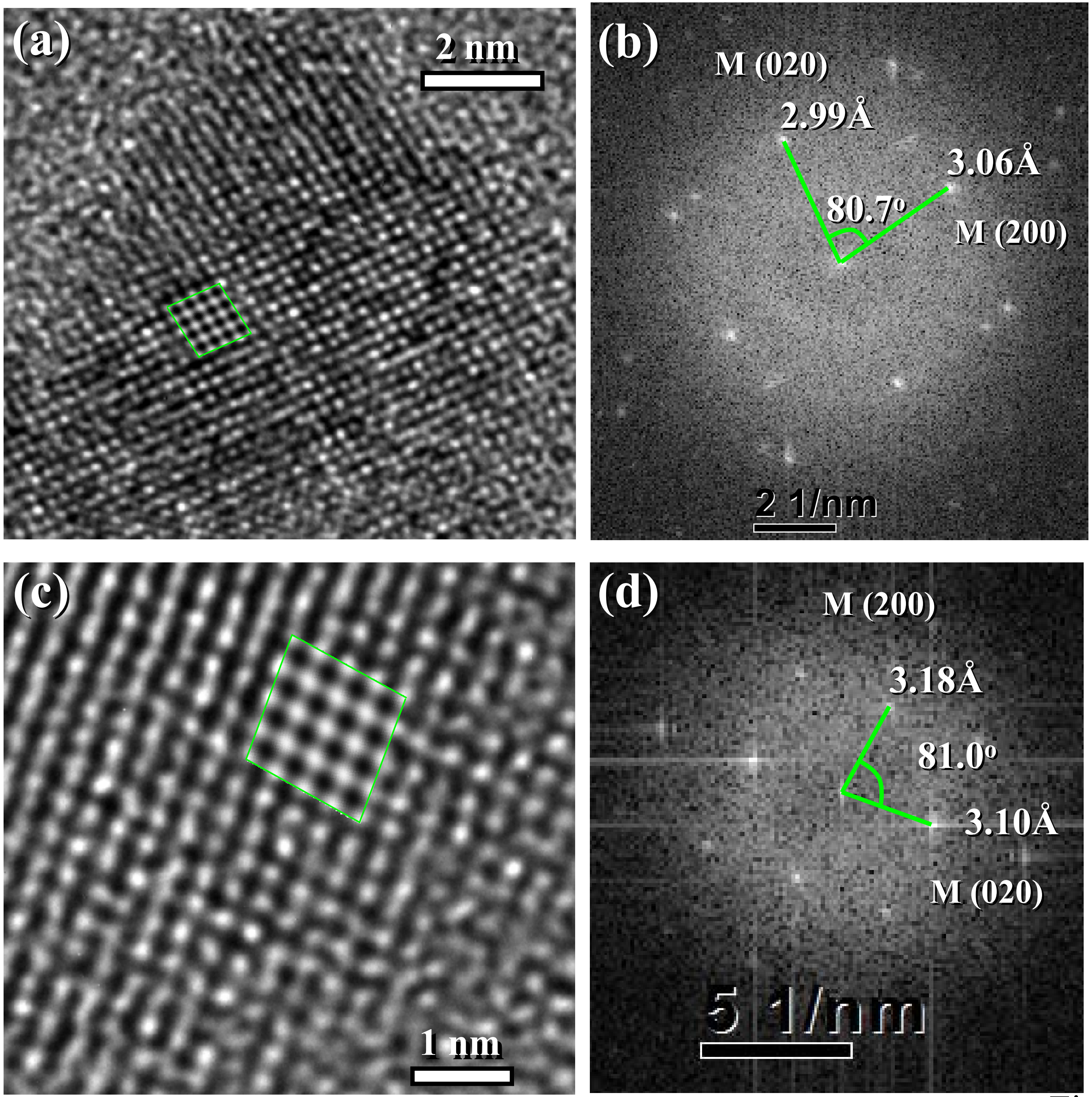

Fig. S2 Jang *et al*.

Figure S3

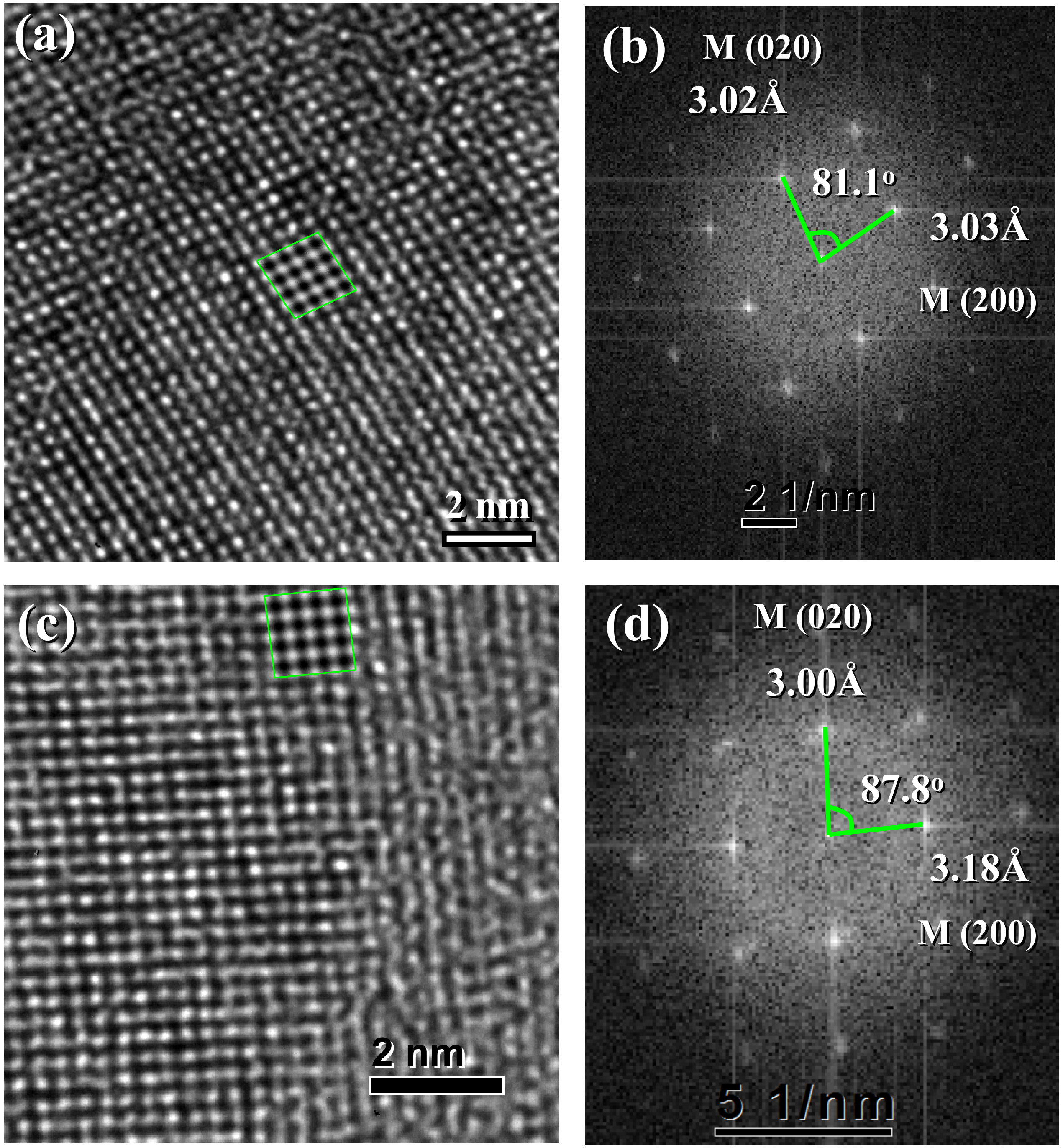

Fig. S3 Jang *et al*.

Figure S4

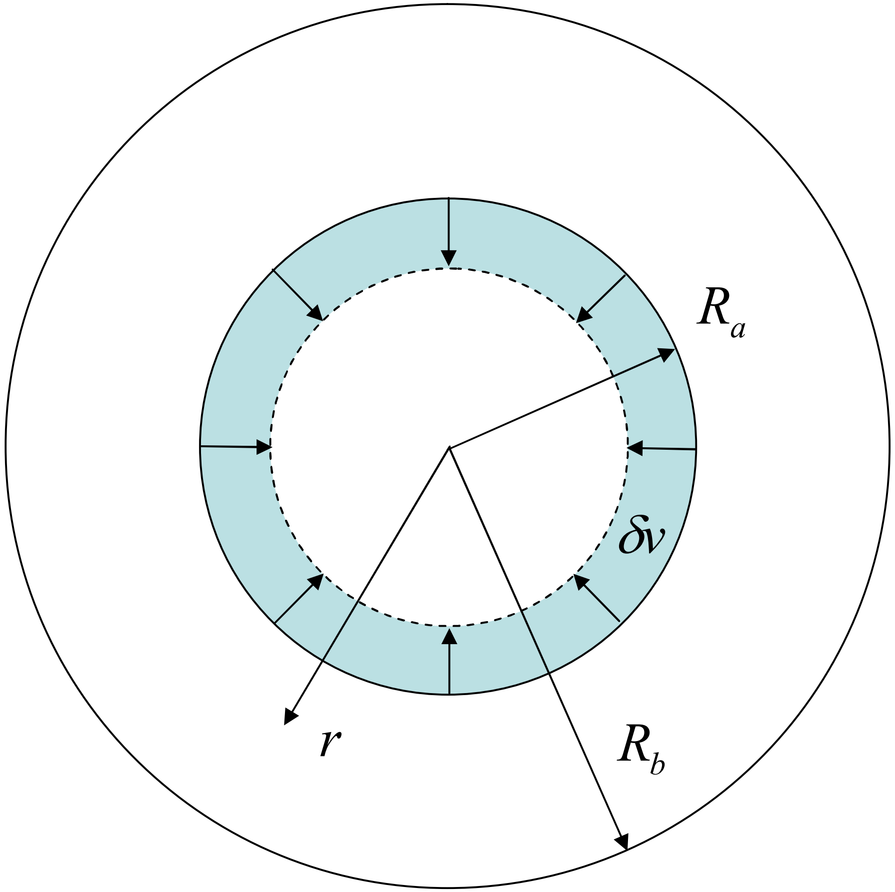

Fig. S4 Jang *et al*.

Figure S5

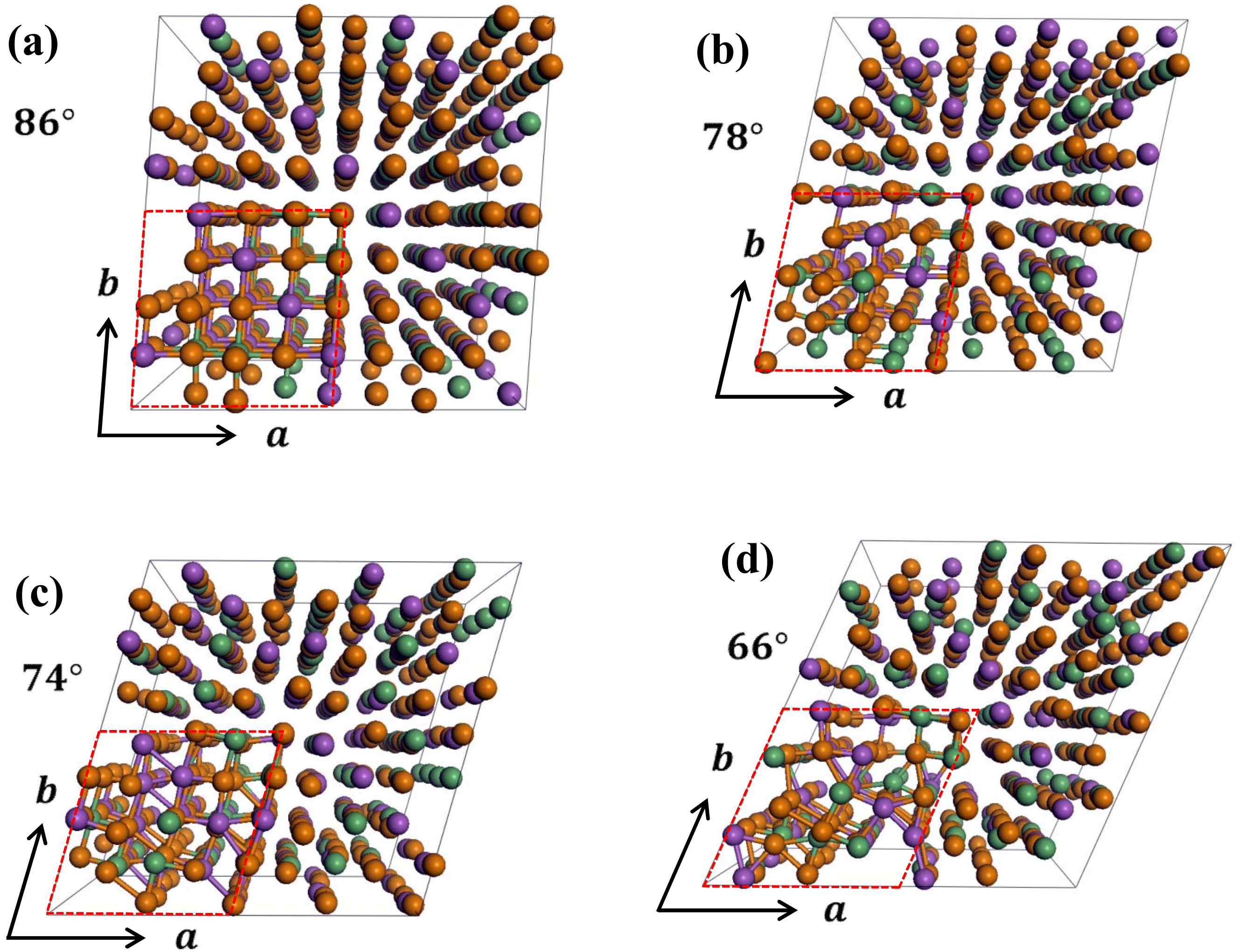

Fig. S5 Jang *et al*.

Figure S6

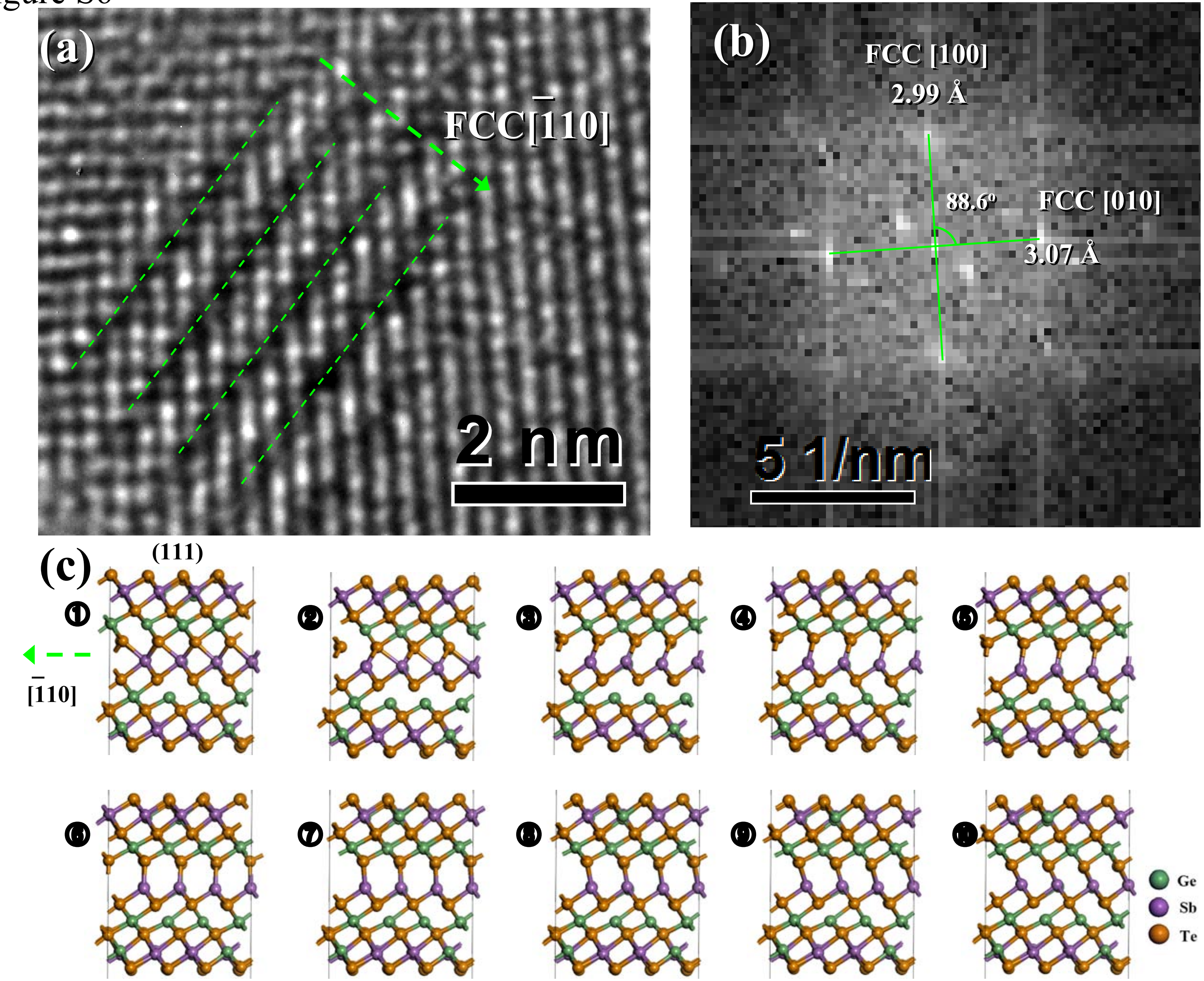

Fig. S6 Jang *et al*.

Figure S7

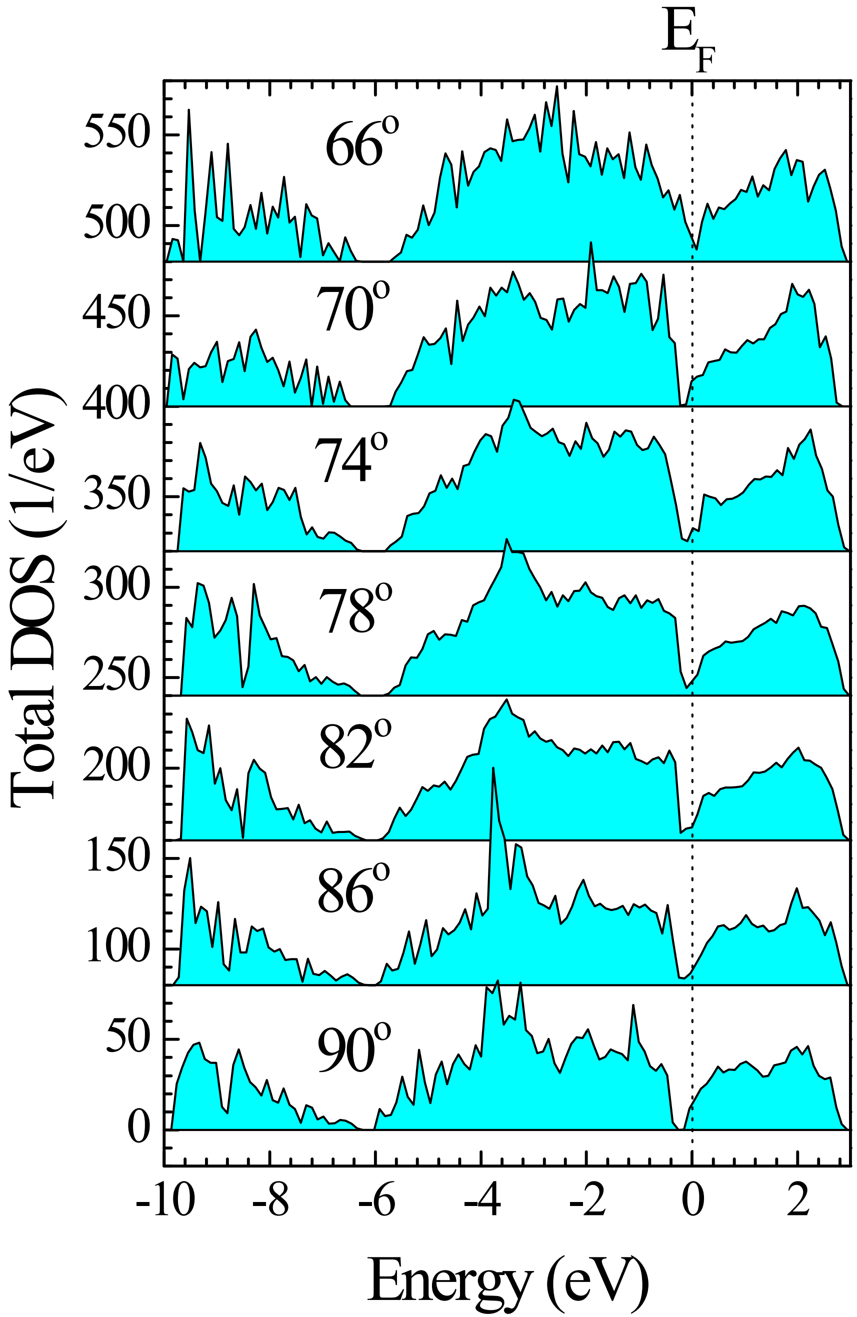

Fig. S7 Jang *et al*.